Heterogeneity of Polyelectrolyte Diffusion in Polyelectrolyte−Protein Coacervates: A ^{1}H Pulsed Field Gradient NMR Study

Amrish R. Menjoge,[†] A. Basak Kayitmazer,[‡,#] Paul L. Dubin,[‡] Werner Jaeger,[§] and Sergey Vasenkov*[,†]

Department of Chemical Engineering, University of Florida, Gainesville, Florida 32611, Department of Chemistry, University of Massachusetts Amherst, Massachusetts 01003, and Fraunhofer Institute of Applied Polymer Research, D-14476 Potsdam-Golm, Germany

Received: December 6, 2007; In Final Form: February 8, 2008

Proton pulsed field gradient (PFG) NMR was used to study the diffusion of poly(diallyldimethylammonium chloride) (PDADMAC) in coacervates formed from this polycation and the protein bovine serum albumin (BSA). Application of high (up to 30 T/m) magnetic field gradients in PFG NMR measurements allowed probing the diffusion of PDADMAC on a length scale of displacements as small as 100 nm in coacervates formed at different pH's and ionic strengths, i.e., conditions of varying protein−polycation interaction energy. Studies were carried out for a broad range of diffusion times and corresponding values of the mean square displacements. Several ensembles of PDADMAC polycations with different diffusivities were observed in the measured range of diffusion times. The existence of these ensembles and the pattern of their changes with increasing diffusion time support the hypothesis about the microscopic heterogeneity of PDADMAC−BSA coacervates and also provide evidence for the dynamic disintegration and reformation of dense domains.

Introduction

Polyelectrolyte−protein coacervation is a special case of complex coacervation wherein a macromolecular solution composed of a protein and an oppositely charged polyelectrolyte forms a metastable biphasic suspension as a result of electrostatic interactions and the entropy gained from small-ion release. Upon centrifugation, this suspension separates into two liquid phases: a dense phase (coacervate), which is rich in protein and polyelectrolyte, and a dilute solution phase, which contains an equilibrium mixture of protein and polyelectrolyte. The latter phase can either be molecularly dispersed or exist in some state of soluble aggregation. Until recently, most studies on protein−polyelectrolyte coacervation focused on various applications such as microencapsulation of active food components,[1,2] pharmaceutical agents,[3] or enzymes,[4] as well as on selective protein separation.[5] Such investigations have often involved protein mixtures (e.g., whey protein) and polyelectrolytes (e.g., gum arabic) that are heterogeneous with respect to molecular weight (MW) and/or chemical composition. Due to such polydispersity, experimental observation of true liquid−liquid phase transitions in such systems has been a very challenging task. This polydispersity impedes experimental studies of the effects on coacervate structure of key variables, such as ionic strength, pH, protein charge anisotropy and polymer charge density, charge lability, and chain stiffness, all of which influence protein−polyelectrolyte complexation.[6] However, even with polydisperse polyelectrolytes, it is possible to observe full retention of activity for enzymes confined in coacervate droplets, confirming not only the preservation of protein structure but also a level of diffusional mobility far in excess of that predicted from coacervate viscosity.[7]

Recent studies of coacervates formed from a well-characterized, structurally homogeneous globular protein (bovine serum albumin (BSA)) and a narrow molecular weight distribution cationic polyelectrolyte (poly(diallyldimethylammonium chloride) (PDADMAC))[8] have provided new information about the dynamics and structure of protein−polyelectrolyte coacervates. Among these findings are the following: (i) multiple diffusion modes of proteins observed by both dynamic light scattering (DLS)[8] and fluorescence recovery after photobleaching (FRAP),[9] (ii) a large fraction of "fast" proteins with diffusivity only 6 times smaller than the corresponding diffusion coefficient in a dilute protein solution,[8] (iii) rheological behavior indicative of a tenuous solid-like network at a low strain, prone to disruption with increasing shear,[8] and (iv) dense (protein-rich) domains observed by cryo-TEM on length scales between tens and hundreds of nanometers.[9] The existence of such domains was found to be consistent with Guinier analysis of static light scattering.[8,9] All these observations point to mesophase separation within the coacervate (i.e., phase separation on the length scale in the order of 1 μm or less), leading to the existence of protein-rich microdomains suspended in a continuous phase with a lower protein concentration.[9] The hypothesis about such mesophase separation finds additional support from the results of small-angle neutron scattering studies.[10]

Although it might be assumed that the electrostatic interactions in coacervates would guarantee that differences in concentration of negatively charged proteins between different types of domains would be mirrored by those of polycations, no direct data about structural and diffusional heterogeneity of polyelectrolytes in coacervates have been reported, primarily because proteins tend to dominate the signal in most scattering experiments. In this paper we present such data for the diffusion

* To whom correspondence should be addressed. Phone: +1 352-392-0315. Fax: +1 352-392-0315. E-mail: svasenkov@che.ufl.edu.
[†] University of Florida.
[‡] University of Massachusetts Amherst.
[§] Fraunhofer Institute of Applied Polymer Research.
[#] Present address: Biomedical Engineering, Northwestern University, Evanston, Illinois 60208.

10.1021/jp711515h CCC: $40.75
Published on Web 03/29/2008

TABLE 1: Samples Used for Proton NMR Studies

sample	type	PDADMAC molecular weight M_w (kDa) and (M_w/M_n)	pH	ionic strength (mM)
A1	BSA		~7	100
A2	BSA−PDADMAC	700 (1.55)	7.7	100
A3	BSA−PDADMAC	219 (1.52)	8.5	100
A11	BSA−PDADMAC	219 (1.52)	9.0	50

of PDADMAC in PDADMAC−BSA coacervates. The diffusion studies were carried out by pulsed field gradient (PFG) NMR, also known as pulsed gradient spin echo (PGSE) NMR.[11,12] This technique can be used for probing diffusion in complex systems for a very broad range of time and length scales, i.e., usually between ca. 10 ms and several seconds and from a fraction of a micrometer to dozens of micrometers, respectively (see, for example, refs 13−20). Spatial resolution of this technique is primarily determined by the maximum achievable strength of the magnetic field gradients.[11,12] Application of stronger gradients allows the use of smaller diffusion times in the measurements and thus leads to an improvement of the spatial resolution.

The PFG NMR technique was previously applied for measurements of diffusivities of polyelectrolytes in coacervates,[13] but only with gradients of relatively small strength (0.5 T/m), which limits spatial resolution. Hence, no data on diffusion heterogeneity over small length scales were reported. In the present study, PFG NMR diffusion measurements were carried out with large (up to 30 T/m) gradients, allowing observation of displacement-dependent polyelectrolyte transport properties in coacervates on the submicrometer length scale, in a manner similar to recent PFG NMR studies of the diffusion of guest molecules on submicrometer length scale in nanoporous materials.[17]

Experimental Section

Materials. PDADMAC of $M_w = 219$ kDa ($M_n = 141$ kDa) and $M_w = 700$ kDa ($M_n = 460$ kDa) samples were prepared by free-radical aqueous polymerization of diallyldimethylammonium chloride[21] and characterized after dialysis and lyophilization by membrane osmometry and light scattering. BSA ($M_w \approx 68$ kDa) with total fatty acid content ≤1.2 mg/g was purchased from Roche Diagnostics (Indianapolis, IN). Deuterium oxide (D_2O, 99.8%) was purchased from Cambridge Isotope Laboratories, Inc. (Andover, MA). The 0.1 and 1 N HCl and NaOH solutions were obtained from Fisher Scientific. Milli-Q water was used in the preparations of all samples.

Preparation of Coacervate Samples. BSA and PDADMAC were dissolved separately in 0.05−0.1 M NaCl solution to give stock solutions of 6 and 1.2 g/L, respectively. Each stock solution was then filtered individually (0.20 μm cellulose acetate, Sartorius Inc.), and the pH of each solution was adjusted to 4.0 (noninteracting conditions) with 0.1 N HCl. Equal volumes of BSA and PDADMAC solutions were mixed to give an initial protein/polymer weight ratio (r) of 5, and the pH of the mixture was adjusted to the desired pH by gradual addition of 0.1 N NaOH and 1 N NaOH. The mixture was centrifuged for 30 min at 4000 rpm at room temperature, and the upper clear solution (supernatant) was removed by pipet from the lower optically clear and viscous fluid (coacervate). Centrifugation was repeated several times to ensure full removal of supernatant. NMR studies were performed with three BSA−PDADMAC coacervate samples (Table 1). In addition, NMR spectra of a sample containing only BSA (i.e., sample A1 in Table 1) were recorded to ensure the proper assignment of NMR lines to BSA or PDADMAC. The relative amounts of BSA in the pure protein sample and that in the coacervate samples were essentially the same, i.e., ~20% protein by weight. In order to minimize the proton NMR signal of water, H_2O in the coacervates was repeatedly exchanged by D_2O to attain a level of 90% v/v D_2O as discussed in ref 10.

NMR Studies. Proton PFG NMR diffusion studies were carried out using a wide-bore Bruker BioSpin spectrometer operating at a ^1H resonance frequency of 750 MHz. High (up to 30 T/m) magnetic field gradients were generated using a *diff60* diffusion probe and *Great60* amplifier (Bruker BioSpin). Diffusion measurements were performed for a broad range of diffusion times (between around 30 and 200 ms) using the PFG NMR stimulated echo sequence.[11,12] Each PFG NMR attenuation curve was obtained by measuring the signal intensity as a function of the amplitude of the magnetic field gradients (g) and keeping all other parameters of the stimulated echo sequence the same. The total measurement time needed to measure one attenuation curve was larger than 1 h for all samples. The signal intensity $A(g)$ at different gradient strengths was obtained by calculating the area under the selected lines of frequency-domain NMR spectra. For each attenuation curve the same integration range on the frequency scale was used.

In the simplest case, when all molecules or ions in a sample exhibit normal (i.e., Fickian) diffusion with a single diffusion coefficient (D), the attenuation curves can be described as[11,12]

$$\Psi \equiv \frac{A(g)}{A(g=0)} = \exp(-1/6(\gamma\delta g)^2\langle r^2(t_{\text{eff}})\rangle) = \exp(-(\gamma\delta g)^2 D t_{\text{eff}}) \quad (1)$$

where $\langle r^2(t_{\text{eff}})\rangle$ is the measured mean square displacement (MSD), δ denotes the effective duration of the gradient pulses, t_{eff} is the effective diffusion time, and γ is the gyromagnetic ratio. The expression in the right-hand part of eq 1 was obtained using the Einstein relation

$$\langle r^2(t_{\text{eff}})\rangle = 6Dt_{\text{eff}} \quad (2)$$

For the PFG NMR stimulated echo sequence and for normal diffusion, $t_{\text{eff}} = \Delta - \delta/3$, where Δ denotes a separation between the gradient pulses. Diffusivities in the studied coacervate samples were obtained by fitting the measured attenuation curves using an equation of the type of eq 1 with several weighted exponential terms corresponding to distinct ensembles of diffusing species with different diffusivities:

$$\Psi = \sum_\alpha A_\alpha \exp(-(\gamma\delta g)^2 D_\alpha t_{\text{eff}}) \quad (3)$$

where A_α and D_α denote the fraction and diffusivity of an ensemble α, respectively. Under our experimental conditions, δ was always much smaller than the effective diffusion time, i.e., $t_{\text{eff}} \approx \Delta$. The effective diffusion time was varied by changing the separation between the second and third $\pi/2$ pulses (τ_2) of the PFG NMR stimulated echo sequence and keeping all other parameters of the sequence constant. In these measurements δ was equal to 3.43 ms, and the separation between the first and the second $\pi/2$ pulses (τ_1) was equal to 4.4 ms. In addition, several measurements were performed with $\tau_1 = 3.9$ ms and $\delta = 2.9$ ms to verify that for a given diffusion time the measured diffusivities are independent of the value of τ_1. The experimentally observed lack of such dependence confirmed that our data are not distorted by the magnetic susceptibility effects.[18] All

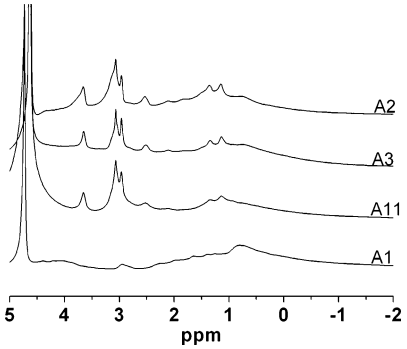

Figure 1. ^{1}H NMR frequency-domain spectra of samples A1, A2, A3, and A11 obtained from the free induction decay (FID) signal.

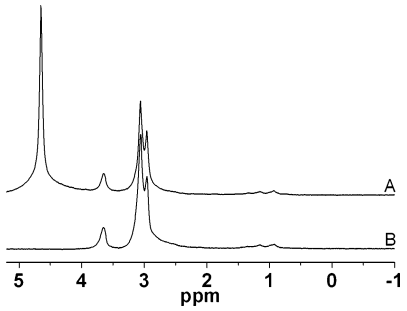

Figure 2. ^{1}H NMR spectra of sample A11 obtained by the PFG NMR stimulated echo pulse sequence for $t_{eff} = 28.85$ ms and the following two gradient strengths: 0.4 (A) and 13 T/m (B). The relative intensity of (B) has been significantly increased to facilitate the comparison of the shape of the spectra. Note the disappearance of the water signal at around 4.6 ppm in the spectrum B corresponding to large gradient strength.

measurements were performed at room temperature (293 K) to avoid occurrence of disturbing convection effects.

Results and Discussion

Figure 1 shows the frequency-domain ^{1}H NMR spectra recorded by the free induction decay (FID) sequence for the samples listed in Table 1. The strong line at about 4.6 ppm is assigned to H_2O. The half-width of this line is significantly smaller in the pure protein sample (A1) than in the coacervate samples. This can be attributed to a lower mobility of water in the latter samples. The broad feature between 2 and 0 ppm in the spectrum of the pure BSA sample is attributed to the protein since the only non-BSA line that we can expect to see in this sample is the water line at around 4.6 ppm. The lines between 4 and 0 ppm in the spectra of coacervate samples A2, A3, and A11 originate from both polyelectrolyte and protein. Comparison of these lines with the spectrum of A1 indicates that the strongest polyelectrolyte lines, with no or little overlap with the water and/or protein lines, are located in the region between 4 and 2 ppm. These lines can be assigned to the *N*-methyl protons and the CH_2 protons of the five-membered rings of PDADMAC.

Comparison of the frequency-domain spectra recorded by the PFG NMR stimulated echo pulse sequence for $g \geq 0$ (see, for example, spectra in Figure 2) with those in Figure 1 revealed that the broad feature in the range between 2 and 0 ppm (Figure 1), assigned to the protein, has completely vanished from the coacervate spectra obtained by the PFG NMR sequence. This effect is attributed to the short NMR transverse relaxation time ($T_2 < 1$ ms), which was estimated from the results of the measurements of the protein signal in the coacervate samples using FID and the stimulated echo sequence. Under conditions of the application of the stimulated echo sequence, the duration

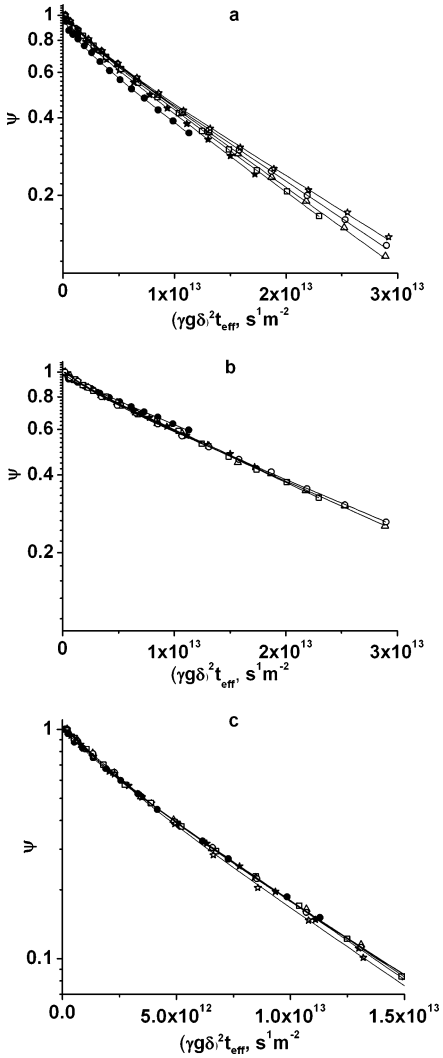

Figure 3. ^{1}H PFG NMR attenuation curves for diffusion of PDADMAC in the coacervate samples A2 (a), A11 (b), and A3 (c). The curves were measured for the following effective diffusion times: 28.85 (●), 43.85 (★), 58.85 (□), 73.85 (△), 98.85 (○), and 198.85 ms (☆). The attenuation range for small diffusion times could not be expanded beyond that shown in the figure because larger duration and/or amplitude of the gradients, which is required to achieve larger attenuation, would lead to overheating of the gradient coil.

of the signal decay with time constant T_2 cannot be smaller than the value of 2δ, here equal to around 7 ms. As a result, no visible protein lines were recorded by this sequence under the measurement conditions. It was verified that even for values of δ much smaller than 3.4 ms but still suitable for diffusion measurements the PFG NMR stimulated echo sequence fails to detect sufficiently strong protein lines. Hence, only diffusion data for PDADMAC are reported.

The attenuation curves for PDADMAC were obtained by integrating the frequency-domain spectra in the range between 3.8 and 1.8 ppm and plotting the resulting integral values as a function of g^2 (Figure 3). In this frequency range, PDADMAC lines do not show a significant overlap with the strong water line. In order to further suppress the influence of water on the measured attenuation curves, we used gradients in the range of 0.4 T/m as the starting, viz., smallest, value. It was observed that such gradients do not lead to any measurable decay of the PDADMAC lines. However, the intensity of the residual water line was sufficiently suppressed so that there was essentially no influence of water on the frequency-domain spectra in the measured range (3.8−1.8 ppm).

TABLE 2: Results of Fitting of the PFG NMR Attenuation Curves Shown in Figure 3 for Coacervate Samples A1, A3, and A11[a]

sample	t_{eff}, ms	fraction a (A_a)	D_a, m^2/s	fraction b (A_b)	D_b, m^2/s	fraction c (A_c)	D_c, m^2/s
A2	28.85	0.11	5.93×10^{-12}	0.09	7.08×10^{-13}	0.79	9.49×10^{-14}
	43.85	0.06	4.17×10^{-12}	0.08	6.83×10^{-13}	0.86	9.30×10^{-14}
	58.85	N/A	N/A	0.12	6.75×10^{-13}	0.88	8.96×10^{-14}
	73.85	N/A	N/A	0.13	6.39×10^{-13}	0.87	8.70×10^{-14}
	98.85	N/A	N/A	0.16	4.89×10^{-13}	0.84	8.13×10^{-14}
	198.85	N/A	N/A	0.19	3.99×10^{-13}	0.81	7.60×10^{-14}
A3	28.85	0.03	6.44×10^{-12}	0.17	7.32×10^{-13}	0.8	1.87×10^{-13}
	43.85	N/A	N/A	0.18	8.36×10^{-13}	0.82	1.92×10^{-13}
	58.85	N/A	N/A	0.22	7.18×10^{-13}	0.78	1.85×10^{-13}
	73.85	N/A	N/A	0.28	5.74×10^{-13}	0.72	1.77×10^{-13}
	98.85	N/A	N/A	0.29	5.36×10^{-13}	0.71	1.76×10^{-13}
	198.85	N/A	N/A	0.25	6.14×10^{-13}	0.75	1.89×10^{-13}
A11	28.85	0.05	4.65×10^{-12}	0.03	4.88×10^{-13}	0.92	4.91×10^{-14}
	43.85	N/A	N/A	0.06	5.67×10^{-13}	0.94	5.53×10^{-14}
	58.85	N/A	N/A	0.07	6.10×10^{-13}	0.93	5.64×10^{-14}
	73.85	N/A	N/A	0.09	4.92×10^{-13}	0.91	5.43×10^{-14}
	98.85	N/A	N/A	0.12	4.19×10^{-13}	0.88	5.13×10^{-14}

[a] Eq 3 with either two or three exponential terms corresponding to PDADMAC ensembles with different diffusivities was used to fit the curves.

In order to further verify that the attenuation curves shown in Figure 3 correspond to the diffusion of PDADMAC only, the shapes of the frequency-domain spectra were compared at various gradient strengths, including those corresponding to the fast initial decay of ψ measured at small diffusion times (Figure 3). The shapes of the spectra provide information on the relationship between the apparent amplitude, the line width, and the integral under the three lines in the range between 3.8 and 1.8 ppm. It was observed that these shapes, and hence also the PFG NMR attenuation curves for different lines, remained the same within the experimental uncertainty. Figure 2 shows an example of such shape comparison for two very different gradient strengths.

The attenuation curves in Figure 3 show non-monoexponential behavior. The diminution of deviations from monoexponential behavior in the initial part of the attenuation curves with increasing diffusion time corresponds mainly to the gradual disappearance of the fast initial decay. However, even for large diffusion times (around 100 ms) the attenuation curves remain noticeably non-monoexponential. Such behavior was observed for all three samples. In general, monoexponential behavior of PFG NMR attenuation curves corresponds to the existence of a single diffusivity for all diffusing species under study (eq 1). Deviations from the monoexponential behavior indicate that there is a distribution of diffusivities. Hence, the data in Figure 3 suggest that there are different ensembles of PDADMAC ions with different effective diffusivities in the coacervate samples.

Changes in the shape of the attenuation curves in Figure 3 with increasing diffusion time can arise from changing relative contributions of different ensembles of PDADMAC ions to the measured signal. This can happen if the characteristic longitudinal NMR relaxation times (T_1) vary for PDADMAC ensembles with different diffusivities and, in addition, if these relaxation times are comparable with the diffusion times used in the measurements. In such case, the contribution of ensembles with smaller T_1 to the measured stimulated echo signal relative to those corresponding to larger T_1 would decrease with increasing diffusion time.[11,12] As a result, the NMR signal of PDADMAC has to become smaller with increasing diffusion time. However, for the measured range of diffusion times, no significant reduction of the signal amplitude with increasing diffusion time was observed. Hence, we can conclude that the characteristic T_1 times are significantly larger than the diffusion times used, and the observed changes of the PFG NMR attenuation curves with increasing diffusion time were not due to the effects of T_1 relaxation.

In order to obtain quantitative information about PDADMAC diffusion the measured attenuation curves were fitted assuming the existence of several ensembles of PDADMAC ions having different diffusivities. In this case, the weighted sum of several exponential terms corresponding to PDADMAC ensembles with different diffusivities (eq 3) was used to fit the data. Fitting the attenuation curves revealed that the minimum number of the exponential terms in eq 3 is two for large diffusion times and three for small diffusion times.

The resulting best-fit values of the diffusivities and the corresponding fractions of PDADMAC ions are presented in Table 2. This table shows that ensembles a and b with large diffusivities represent only a small fraction of all PDADMAC ions contributing to the measured NMR signal, an unexpected result since for the protein the large diffusivity mode was elsewhere (ref 8) observed to be the dominant one. In comparison, at least 70% of the measured PDADMAC signal corresponds to the slowest component, c. The diffusivity of the slowest component remains mostly the same with increasing diffusion time, and its relative contribution shows some tendency to decrease slowly with increasing time (Table 2). This decrease in the fraction of c is compensated by the corresponding increase in the fraction of component b. Table 2 shows that the latter fraction increases very significantly in the measured range of diffusion times. Such behavior can be tentatively interpreted as a manifestation of exchange between these two fractions.

Figure 4 shows dependencies of the diffusivities of the different ensembles of PDADMAC ions on the root-mean-square displacements (MSD) obtained using the Einstein relation (eq 2). This figure demonstrates that the application of high magnetic field gradients allowed us to probe diffusion of PDADMAC on the length scale of displacements smaller than 100 nm for fraction c. Increase in the diffusion time of PFG NMR measurements resulted in an increase in the values of the measured root-mean-square displacements. It is seen in Figure 4 that the diffusivities of fraction c were measured in the range of displacements between ca. 90 and 500 nm, while diffusivities of fractions a and b were measured for displacements up to ca. 1 μm.

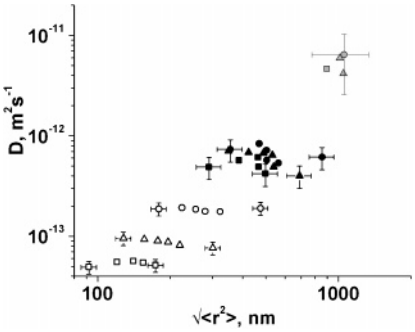

Figure 4. Dependence of the effective diffusivities of PDADMAC shown in Table 1 on the root-mean-square displacements calculated using the Einstein relation (eq 2). Triangles, circles, and squares show diffusivities for the samples A2, A3, and A11, respectively. Fractions a, b, and c are indicated by gray, black, and empty symbols, respectively.

The observation of fast-diffusing PDADMAC fractions (a + b) and a slow-diffusing fraction (c) can be discussed in relation to recent results, which suggest the existence of two different types of domains in the coacervate samples: dense microdomains with a high concentration of BSA and dilute domains with a low concentration of BSA. Limited cryo-TEM images of BSA−PDADMAC coacervates[9,10] suggest that dilute domains form a continuous phase with volume fraction of ca. 0.85. This estimate is in agreement with the observation that the fast-diffusing component of BSA recorded by DLS in BSA−PDADMAC coacervates corresponds to around 75% of total BSA.

Protein−polyelectrolyte coacervate morphology suggested by cryo-TEM involves irregular and partially interconnected solid-like regions with sizes between 100 and 1000 nm. In other systems exhibiting similar morphologies, viz., colloidal solutions of weakly charged colloidal silver[22] and Boehmide rods,[23] mesophase separation appears to arise from a combination of short-range attraction and long-range repulsion, which supports the hypothesis that aggregates of protein−polyelectrolyte on the order of 50 nm, and with residual net charge, can form clusters in the range of hundreds to thousands of nanometers. This scenario is consistent with the cryo-TEM and small-angle neutron scattering (SANS) data for the BSA/PDADMAC system[9,10] and with SANS and electron microscopy data for the lysozyme/poly(styrene sulfonate) system.[24] It has further been proposed[25] that Lys−NaPSS complexes phase separating from water consist of dense polyelectrolyte−protein "globules" (a.k.a. aggregates) of 30−40 nm in diameter separated by ca. 10 nm domains. These interaggregate regions consist of polyelectrolyte chains and their counterions when the polyelectrolyte/protein charge ratio is 2−3 (this ratio is 4 for the coacervates of the present study) and are thus intracluster spaces from which excess polyelectrolyte can be released (see below). It is expected that the rotational and conformational mobility of PDADMAC ions in the static aggregates and in the intracluster spaces between aggregates is significantly reduced in comparison to the dilute phase.[8] As a result, rotation and/or change of conformation of PDADMAC polycations is likely to be too slow on the NMR time scale for averaging out the effect of proton dipole−dipole interaction on the T_2 NMR relaxation time, which is expected to be significantly reduced by such interactions. In particular, a pronounced decrease of proton T_2 NMR relaxation time due to hindered mobility of PDADMAC in related systems was recently reported in ref 26. It is likely that the T_2 values of PDADMAC in dense domains are so small that no NMR signal from these PDADMAC polycations can be recorded by the stimulated echo sequence under our experimental conditions. This assumption is in agreement with the observation that the average line width of PDADMAC is larger for the FID measurements (Figure 1) than for the measurements with the stimulated echo sequence by around 3%. In the former measurements the signal of essentially all PDADMAC ions can be recorded while in the latter measurements the PDADMAC signal is reduced due to T_2 NMR relaxation in the same way as discussed above for BSA.

On the basis of the discussion above, it is very likely that our PFG NMR measurements failed to detect PDADMAC ions in dense domains. The largest fraction (c) of PDADMAC ions can be attributed to diffusion in the dilute phase, which is expected to account for around 85% of the sample volume. PDADMAC ions with higher diffusivities (a + b) can be tentatively attributed to those released from a fraction of dense domains which are in the process of breaking up during the time window of diffusion measurements. Recent DLS data suggest that breakup of dense domains can occur on the time scale of dozens of milliseconds.[9] This time scale is comparable with the diffusion time in the PFG NMR measurements (Table 2). A rapid breakup of dense domains can lead to a massive release of PDADMAC ions, with the intracluster regions mentioned above acting as reservoirs for the release of excess PDADMAC. Once released, the PDADMAC ions are expected to move freely away from the newly created boundaries between dense and dilute domains. The effective diffusivity of the released PDADMAC at such boundaries can be larger than that in dilute domains far from the boundaries because the release of PDADMAC is expected to lead to a concentration gradient at the domain boundaries and hence short-range flow of PDADMAC into dilute domains. The existence of such flows can significantly increase effective diffusivity of PDADMAC because this diffusivity is determined from the measured MSD values using eq 2. For a sufficiently strong, homogeneous flow the effective diffusivity can be estimated as

$$D = \frac{1}{6t_{\mathrm{eff}}}\langle r^2(t_{\mathrm{eff}})\rangle \approx \frac{1}{6t_{\mathrm{eff}}}\left(\int_0^{t_{\mathrm{eff}}} v(t)\,\mathrm{d}t\right)^2 \qquad (4)$$

where it was assumed that all PDADMAC ions move with the same velocity equal to the flow velocity $v(t)$. In the coacervate samples a characteristic velocity of the PDADMAC flows is expected to become smaller with time because of leveling off of the concentration gradients. Consequently, the effective diffusivity as a function of time is expected to grow more slowly than the linear dependence given by eq 4 with a time-independent velocity. The diffusivity can even remain almost constant or decrease with increasing time. This expectation is in agreement with the results for the PDADMAC component b in Table 1 which does not show any significant dependence of the diffusivity of this component on diffusion time. The short-range flows discussed above are bound to include and carry with them some of the PDADMAC polycations located in the dilute domains near boundaries. Inclusion of polyelectrolyte from dilute domains into the flows explains why with increasing diffusion time, the fraction of rapidly diffusing component b increases and the fraction of c decreases (Table 1).

A reduction in the volume of dense domains due to their breakup has to be compensated by new dense domain formation since the total volume of dense domains is expected to remain constant under the conditions of our measurements. Under these conditions the macroscopic NMR samples are expected to be in a steady state characterized by a constant free energy and the related constant volume fraction of dense domains because

the sample was kept at the same temperature for at least several days before the measurements. Formation of dense domains within dilute domains can lead to transient local decrease in the concentration of PDADMAC and BSA in the dilute phase as these macroions are consumed in the process of dense domain formation. The latter is likely to lead to short-range flows and to the corresponding increase of the polyelectrolyte fractions with high effective diffusivities as measured by PFG NMR. Based on the discussion above we can conclude that the PFG NMR detection of highly mobile polyelectrolyte components a and b can be tentatively attributed to both breakup and formation of dense domains.

Previous studies of PDADMAC−BSA coacervates using DLS and FRAP suggest that the stability of dense domains, i.e., the characteristic time scale of domain breakup, depends on the pH and ionic strength of the coacervate samples.[8,9] Under the conditions of strong interactions in the coacervates characterized by high pH and low ionic strength (sample A11), large and stable dense domains are expected to exist. In contrast, dense domains in coacervates prepared at low pH and high ionic strength are expected to be less stable (sample A3). These expectations are consistent with the data in Table 2 showing that the sum of the relative contributions of components a and b, which are attributed to the processes of breakup and formation of dense domains, is about twice as large for A3 than for A11 for all diffusion times used. The remaining sample A2 is also characterized by low pH and high ionic strength. However, the polyelectrolyte molecular weight for A2 is significantly larger, which is expected to lead to a reduced rate of domain breakup. This is in agreement with the observation that the sum of the fractions of the components a and b in A2 is slightly smaller than that in A3.

In addition to the stability of dense domains discussed above, ion diffusivities in the dilute phase can also show some dependence on coacervate pH and ionic strength. In particular, DLS data suggest that the diffusivity of BSA assigned to dilute domains in sample A3 (low pH, high ionic strength) is almost a factor of 2 higher than that in sample A11 (high pH, low ionic strength).[9] This is in qualitative agreement with the observation that the polyelectrolyte diffusivity inside dilute domains, which are not affected by the short-range flows, is larger in A3 than in A11 (compare data for fraction c in Table 2 and in Figure 4).

Conclusions

PFG NMR diffusion studies of PDADMAC polycations in several samples of PDADMAC−BSA coacervates reveal the existence of diffusion heterogeneity for PDADMAC on length scales from ca. 1000 nm down to 100 nm. Such studies become possible due to the application of high (up to 30 T/m) magnetic field gradients. Observation of several ensembles of PDADMAC ions having different diffusivities supports the hypothesis of the existence of microscopic domains in coacervates. The PDADMAC ensemble with the smallest diffusivity is attributed to normal self-diffusion in dilute domains representing ca. 85% of the coacervate volume, whereas the ensembles with large effective diffusivities are tentatively assigned to PDADMAC transport arising from concentration gradient-driven flows in dilute domains. Such flows are believed to occur due to constant breakup and formation of dense domains.

Acknowledgment. NMR data were obtained at the Advanced Magnetic Resonance Imaging and Spectroscopy (AMRIS) facility in the McKnight Brain Institute of the University of Florida. We thank Dr. Dan Plant, AMRIS, for his help with NMR measurements.

References and Notes

(1) Weinbreck, F.; Minor, M.; de Kruif, C. G. *J. Microencapsulation* **2004**, *21*, 667.
(2) Yeo, Y.; Bellas, E.; Firestone, W.; Langer, R.; Kohane, D. S. *J. Agric. Food Chem.* **2005**, *53*, 7518.
(3) Burgess, D. J.; Ponsart, S. *J. Microencapsulation* **1998**, *15*, 569.
(4) Yu, X.; Li, Y.; Wu, D. *J. Chem. Technol. Biotechnol.* **2004**, *79*, 475.
(5) Wang, Y.; Gao, J. Y.; Dubin, P. L. *Biotechnol. Prog.* **1996**, *12*, 356.
(6) Cooper, C. L.; Dubin, P. L.; Kayitmazer, A. B.; Turksen, S. *Curr. Opin. Colloid Interface Sci.* **2005**, *10*, 52.
(7) Xia, J.; Mattison, K.; Romano, V.; Dubin, P. L.; Muhoberac, B. B. *Biopolymers* **1997**, *41*, 359.
(8) Bohidar, H. B.; Dubin, P. L.; Majhi, P. R.; Tribet, C.; Jaeger, W. *Biomacromolecules* **2005**, *6*, 1573.
(9) Kayitmazer, A. B.; Bohidar, H. B.; Mattison, K. W.; Bose, A.; Sarkar, J.; Hashidzume, A.; Russo, P. S.; Jaeger, W.; Dubin, P. L. *Soft Matter* **2007**, *3*, 1064.
(10) Kayitmazer, A. B.; Strand, S. P.; Tribet, C.; Jaeger, W.; Dubin, P. L. *Biomacromolecules* **2007**, *8*, 3568.
(11) Callaghan, P. T. *Principles of NMR Microscopy*; Clarendon Press: Oxford, 1991.
(12) Kärger, J., Ruthven, D. M., Eds. *Diffusion in Zeolites: and Other Microporous Solids*; John Wiley and Sons, Ltd.: New York, 1992.
(13) Weinbreck, F.; Rollema, H. S.; Tromp, R. H.; de Kruif, C. G. *Langmuir* **2004**, *20*, 6389.
(14) Ulrich, K.; Sanders, M.; Vasenkov, S. *Magn. Reson. Imaging* **2007**, *25*, 493.
(15) Taglienti, A.; Cellesi, F.; Crescenzi, V.; Sequi, P.; Valentini, M.; Tirelli, N. *Macromol. Biosci.* **2006**, *6*, 611.
(16) Shahedi, V.; Oraedd, G.; Lindblom, G. *Biophys. J.* **2006**, *91*, 2501.
(17) Kortunov, P.; Vasenkov, S.; Kaerger, J.; Valiullin, R.; Gottschalk, P.; Elia, M. F.; Perez, M.; Stoecker, M.; Drescher, B.; McElhiney, G.; Berger, C.; Glaeser, R.; Weitkamp, J. *J. Am. Chem. Soc.* **2005**, *127*, 13055.
(18) Vasenkov, S.; Galvosas, P.; Geier, O.; Nestle, N.; Stallmach, F.; Kärger, J. *J. Magn. Reson.* **2001**, *149*, 228.
(19) Groger, S.; Rittig, F.; Stallmach, F.; Almdal, K.; Stepanek, P.; Papadakis, C. M. *J. Chem. Phys.* **2002**, *117*, 396.
(20) Griffiths, P. C.; Cheung, A. Y. F.; Davies, J. A.; Paul, A.; Tipples, C. N.; Winnington, A. L. *Magn. Reson. Chem.* **2002**, *40*, S40.
(21) Dautzenberg, H.; Goernitz, E.; Jaeger, W. *Macromol. Chem. Phys.* **1998**, *199*, 1561.
(22) Meyer, M.; Le Ru, E. C.; Etchegoin, P. G. *J. Phys. Chem. B* **2006**, *110*, 6040.
(23) Groenewold, J.; Kegel, W. K. *J. Phys. Chem. B* **2001**, *105*, 11702.
(24) Gummel, J.; Cousin, F.; Verbavatz, J. M.; Boué, F. *J. Phys. Chem. B* **2007**, *111*, 8540.
(25) Gummel, J.; Cousin, F.; Boue, F. *J. Am. Chem. Soc.* **2007**, *129*, 5806.
(26) Kriz, J.; Dybal, J.; Kurkova, D. *J. Phys. Chem. A* **2002**, *106*, 7971.